

Article

Chemical Composition and Strontium Isotope Characteristics of Scheelite from the Doranasai Gold Deposit, NW China: Implications for Ore Genesis

Xun Li ¹, Abulimiti Aibai ², Xiheng He ³ , Rongzhen Tang ¹ and Yanjing Chen ^{1,2,*}

¹ Ministry of Education Key Laboratory of Orogenic Belts and Crustal Evolution, Peking University, Beijing 100871, China; 18510067535@163.com (X.L.); skdtrzh@163.com (R.T.)

² Xinjiang Research Center for Mineral Resources, Xinjiang Institute of Ecology and Geography, Chinese Academy of Sciences, Urumqi 830011, China; ablimitab@ms.xjb.ac.cn

³ State Key Laboratory of Geological Processes and Mineral Resources, China University of Geosciences, Beijing 100083, China; hexiheng@126.com

* Correspondence: yjchen@pku.edu.cn

Abstract: Scheelite, as a common accessory mineral found in hydrothermal deposits, is an indicator that allows the study of the ore-forming hydrothermal process and the tracing of fluid sources. The Doranasai gold deposit is a large-sized orogenic gold deposit in the South Altai, and orebodies occur as veins in the Devonian Tuokesalei Formation and Permian albite granite dykes. The ores are quartz veins and altered tectonites (rocks). Here, scheelite can be observed in the early-stage milky quartz veins, the middle-stage smoky quartz-polymetallic sulfide veins, and the altered albite granite dykes. In this study, the scheelites of these three types were carefully investigated in terms of texture, element, and isotope geochemistry to understand their ore-forming processes and fluid sources. The results showed that all types of scheelite were rich in Sr and poor in Mo, indicating that their ore-forming fluids had no genetic relation to magmatic–hydrothermal activities. The scheelites were characterized by the enrichment of medium rare earth element (MREE) and positive Eu anomaly in the chondrite-standardized REE patterns. This indicated the REE differentiation between scheelite and fluid, i.e., REE³⁺ and Na⁺ were in the form of valence compensation, preferentially replacing Ca²⁺ and selectively entering the scheelite lattice. The trace element composition of scheelite showed that the ore-forming fluid system was relatively closed, mesothermal, Na-rich, and reductive. The Sr isotope ratio of the scheelite (0.704819–0.70860, average 0.706372) was higher than that of the ore-bearing albite granite dyke (0.704654–0.704735), indicating that the Tuokesalei Formation is the main source for the fluids forming the Doranasai deposit.

Keywords: scheelite; chemical composition; in situ Sr isotope; ore-forming fluids; Doranasai gold deposit



Citation: Li, X.; Aibai, A.; He, X.; Tang, R.; Chen, Y. Chemical Composition and Strontium Isotope Characteristics of Scheelite from the Doranasai Gold Deposit, NW China: Implications for Ore Genesis. *Minerals* **2022**, *12*, 637. <https://doi.org/10.3390/min12050637>

Academic Editors: Ryan Mathur, Wenlei Song, Xiaohua Deng and Zhanke Li

Received: 24 April 2022

Accepted: 16 May 2022

Published: 18 May 2022

Publisher's Note: MDPI stays neutral with regard to jurisdictional claims in published maps and institutional affiliations.



Copyright: © 2022 by the authors. Licensee MDPI, Basel, Switzerland. This article is an open access article distributed under the terms and conditions of the Creative Commons Attribution (CC BY) license (<https://creativecommons.org/licenses/by/4.0/>).

1. Introduction

The Doranasai deposit is a large gold deposit located on the southern margin of Altai on the Central Asian Orogenic Belt (CAOB) [1]. Since its discovery, previous studies have focused on the characteristics of its ore geology, ore-controlling structures, ore-forming fluids, and metallogenic ages [1–6]. However, there are two contrasting views on the genetic types of the deposit: (1) the Doranasai gold deposit is closely related to albite granite dyke, and ore-forming fluids mainly come from magmatic fluids [4,6]; (2) according to the fact that orebodies are controlled by faults, some scholars have confirmed that the gold deposit belongs to the orogenic type, and the ore-forming fluids mainly come from metamorphic devolatilization [1,7–9]. Therefore, identifying the nature and source of the ore-forming fluids in the Doranasai gold deposit is the key to understanding ore genesis.

Scheelite is commonly found in hydrothermal deposits such as porphyry–skarn tungsten–molybdenum deposits, quartz vein tungsten deposits, and orogenic gold deposits [10–17], and is widely used as an indicator to study the genesis of hydrothermal

deposits and to trace the source of ore-forming fluids [11,13,15,17–26]. Scheelite is often rich in REE, Sr, Pb, Mo, and other elements because REE³⁺ and Sr²⁺ can substitute Ca²⁺, and Mo⁶⁺ can substitute W⁶⁺ as an isomorphic form and enter the scheelite lattice during crystallization. Thus, trace elements of scheelite always provide significant information to understand the ore-forming process and fluid sources [10,11,13,17,27]. For example, Song et al. (2019) carried out a scheelite Sr isotope study of the Gaojiazhuang porphyry–skarn tungsten deposit in the Anhui Province, which showed that the W-Mo-bearing fluids were mainly sourced from the crust [28].

In this contribution, we present new data obtained from detailed petrographic, elemental, and Sr isotope studies of scheelite samples collected from altered albite granite dykes, early-stage milky quartz veins, and middle-stage quartz–polymetallic sulfide veins occurring in the Doranasai gold deposit, and thereby we discuss the source and evolution of ore-forming fluids and the ore-forming process of the Doranasai gold deposit.

2. Regional Geology

Altai Orogen is situated in the core part of the CAOB (Figure 1a) and comprises magmatic, metamorphic rocks, and ore deposits [29]. The Chinese Altai is in the southern part of Altai Orogen. It includes four tectonic units, namely North Altai, Central Altai, South Altai and the Irtysh Belt, which are divided by the Hongshanzui, Abagong and Kezija'er faults, respectively (Figure 1b) [30]. The stratigraphic units in North Altai include the Upper Devonian Kumasu Formation and the Lower Carboniferous Hongshanzui Formation, which are composed of clastic sedimentary rocks, limestone, and a small proportion of volcanic rocks. The Central Altai is characteristic of the middle–high-grade metamorphic sedimentary rocks of the Sinian- or Neoproterozoic–Middle Ordovician Habahe Group and the low greenschist facies turbidite sequences of Middle Ordovician Kulumuti Formation. The South Altai is composed of volcanic rocks of the Lower Devonian Kangbutiebao Formation and volcanic sedimentary rocks of the Middle Devonian Altay Formation. The Irtysh Belt is covered by the Carboniferous Kala'erqisi Formation [31]. Granitoids account for 40% of the area [32], and are mainly formed at about 400 Ma and 270 Ma [33,34]. Ordovician–Silurian granitoids have calc-alkaline characteristics which are related to oceanic plate subduction, while the Permian alkaline granitoids were mainly formed in the collision to post-collision setting after the closure of the ocean basin [35].

Altai Orogen contains huge amounts of VMS, skarn, and orogenic deposits, and is one of the largest metallogenic belts of Cu-Pb-Zn, Au and rare metals in the CAOB. In the Chinese Altai, Ashele Cu-Pb-Zn deposit, Keketale Pb-Zn deposit, and Mengku Fe skarn deposit were formed in the Paleozoic trench–arc–basin system [30,36,37]. The orogenic gold deposits mainly developed along the 600-kilometre-long Irtysh fault zone and its secondary faults, including the Doranasai, Tokuzbay and Sarbulak deposits [1,38,39] (Figure 1b). These gold deposits are believed to have developed during the Permian continental collision between the Kazakhstan and Mongol–Siberian plates [7,38]. The pegmatite-related rare metal deposits, represented by the Koktokay (Keketuohai) No. 3 Vein, are important ore systems generated during the post-collisional extension setting during the late-stage evolution of the CAOB [40].

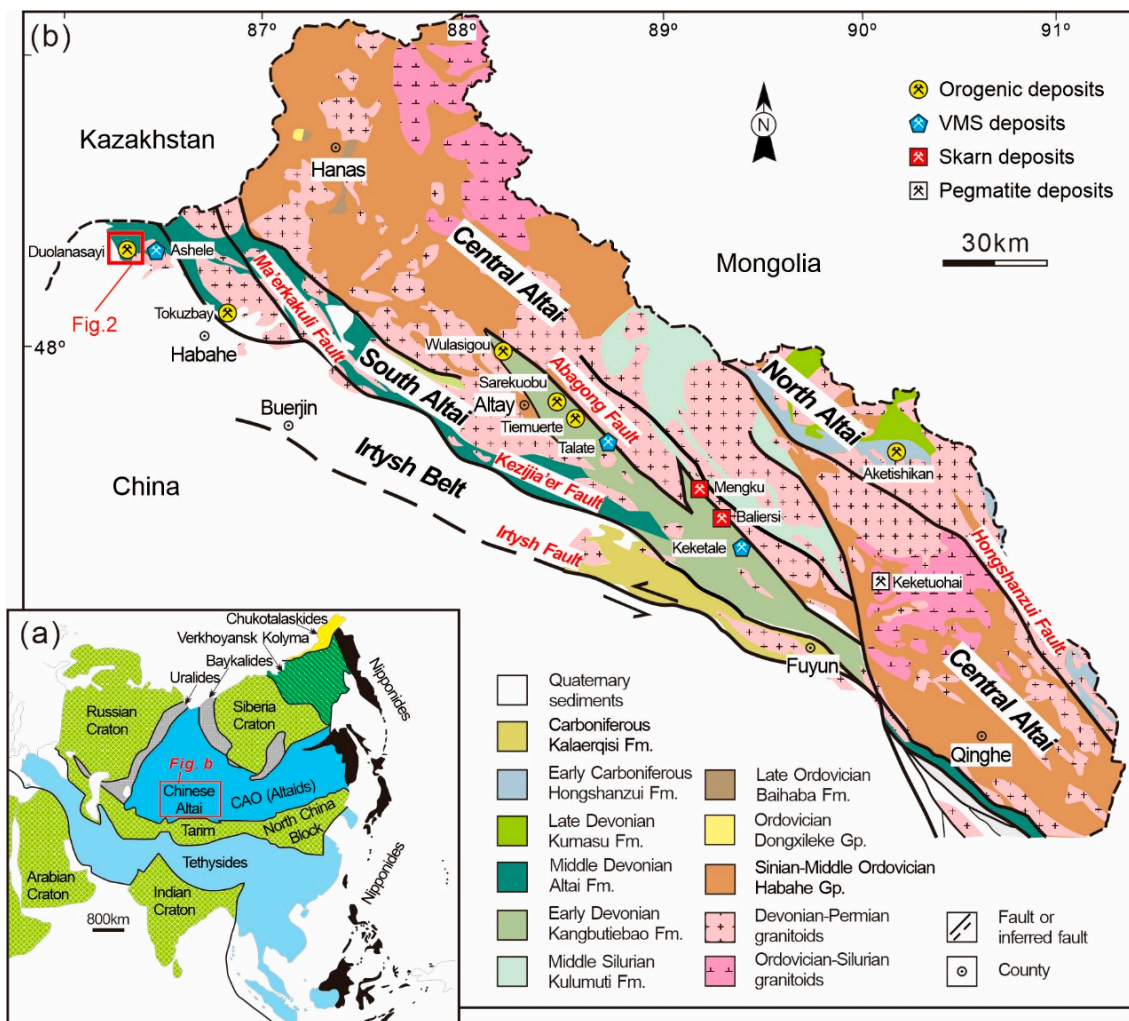


Figure 1. Geological map of the Chinese Altai Orogen, showing the distribution of ore deposits ((a), modified after [29]; (b), modified after [30], reproduction with permission from F.Q. Yang).

3. Deposit Geology

3.1. Local Geology

The Doranasai gold deposit is located in the northeast of the Irtysh Belt and on the west side of the Ma'erkakuli Fault in the south part of the Chinese Altai (Figure 1b). The exposed strata in the Doranasai deposit mainly comprise the third lithologic member of the Middle Devonian Tuokesalei Formation (Figure 2a), which is composed of clastic rocks intercalated with carbonate and siliceous rocks. The Tuokesalei Formation includes four members numbered from the bottom to the top [41]. The first member is composed of dark-gray fine sandstones and siltstones, which mainly distribute in the external contact zone of the Donggele pluton in the east, and minor in the northwest. The second member comprises greenish-gray fine sandstone and siltstone intercalated with sericite–chlorite phyllites; it develops well in the east and west of the deposit and is an important layer hosting gold orebodies. The third member consists of dark-gray carbonaceous bioclastic limestones, and constitutes the northeast and southwest wings of the Aksay syncline, respectively. It is also an ore-bearing layer. The fourth member mainly comprises dark-gray carbonaceous phyllites intercalated with marble and siliceous slate lenses, forming the core of the Aksay syncline (Figure 2a).

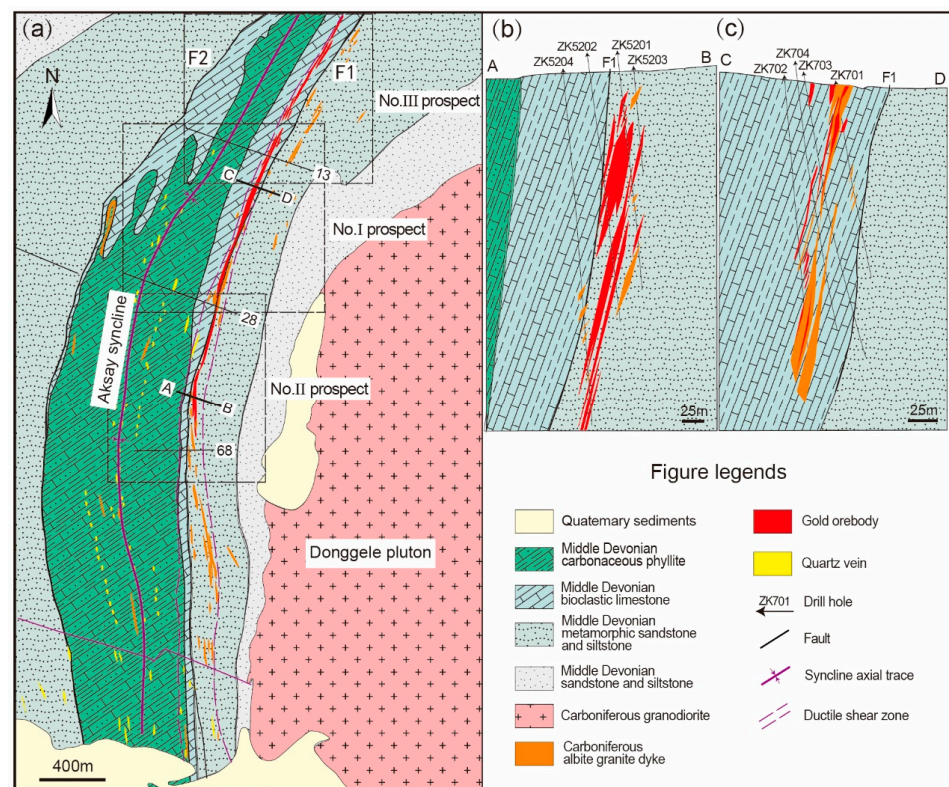


Figure 2. Simplified geological map of the Doranasai gold deposit (reprinted with permission from Ref. [1]). (a) Map showing the spatial relationship of orebodies with syncline, shear zone and granitic rocks; (b) profile showing orebody occurrence in Prospect II; (c) profile showing orebody occurrence in Prospect I.

The Donggele granodiorite is conspicuous in the Doranasai deposit, intruding into the fine-grained sandstone and siltstone of the third lithologic member of the Middle Devonian Tuokesalei Formation (Figure 2a). In mineralogy terms, it is mainly composed of plagioclase, quartz, amphibole, biotite, and accessory minerals such as magnetite, apatite and zircon. A previous study has reported an Rb-Sr isochron age of 289 ± 5 Ma for granodiorite [42]. In addition, several albite granite dykes occur at the deposit. They are NNE-striking, NW-dipping and closely related to gold mineralization [6].

The structures in the Doranasai deposit (Figure 2a) are characterized by the nearly north-to-south-trending Aksay overturned syncline and its associated faults. The Aksay syncline elongates for more than 15 km with a width of 2–3 km. The core of the syncline is carbonaceous phyllite and the two wings are mainly of carbonaceous bioclastic limestone [3]. The faults in the deposit are mainly NNE-trending, followed by NW-trending and near-EW-trending. The F1 fault, located in the center of the deposit, is an interlayer fault between metamorphic sandstone and siltstone and the bioclastic limestone of the Tuokesalei Formation, which is about 5 km long and 20–50 m wide, dipping to NNW with angles of 60–85°. This fault controls the occurrence of orebodies in three prospects (Nos. I, II, and III) and by the emplacement of albite granite dykes [4]. The F2 fault is also an interlayer fault between carbonaceous phyllite and the metamorphic sandstone–siltstone assemblage of the Tuokesalei Formation. It is 5 km long, dipping to NNW with angles of 70–85°.

3.2. Ore Geology

The 28 orebodies of the Doranasai gold deposit occur along fault F1 in the east wing of the Aksay overturned syncline. The ore-bearing altered tectonite zone is about 3 km long from north to south, and is 50–200 m wide. The orebodies are divided into three prospects

from north to south, i.e., No. III, No. I and No. II, respectively. These orebodies yield more than 20 t Au in metal, with an average grade of 5.5 g/t [3].

The No. II prospect of the Doranasai gold deposit contains eight industrial and eight low-grade orebodies controlled by the ductile shear zone [34]. Most orebodies occur in the metamorphic sandstone–siltstone assemblage in the footwall of the shear zone, i.e., the F1 fault (Figure 2b). The main orebody is 260 m long, 0.5–6 m wide, and 250–430 m deep, striking nearly north-to-south and dipping to the west with angles of 78–82°.

The ores of the Doranasai gold deposit mainly include quartz vein and altered rock (tectonite) types [3]. Altered-rock-type ores include altered phyllite, altered sandstone, and altered albite granite dyke. Quartz-vein-type ores mostly occur in the altered albite granite dyke in the form of veins and veinlets. The main ore minerals include pyrite, chalcopyrite, pyrrhotite, galena, sphalerite and scheelite, followed by hematite, cassiterite, molybdenite and tellurite. Gold occurs as natural gold, electrum and calaverite. Gangue minerals include plagioclase, quartz, calcite, dolomite, biotite and rutile. Wall-rock alterations include albitization, pyritization, sericitization, silicification, chloritization and carbonation. Pyritization, sericitization and silicification are the most widespread and closely related to gold mineralization [4], constituting the commonly used term of phyllic alteration.

Based on crosscutting relationships between ore veins and their mineral assemblages, the ore-forming process is divided into three stages [1]: (1) the early-stage quartz–albite vein (Figure 3a–c), in which milky quartz and albite (scheelite \pm pyrite \pm sericite) occur as veinlets, massive blocks and lenticules; (2) the middle-stage quartz–polymetallic sulfide vein (Figure 3d–f), in which quartz presents as fine veins containing various amount of metal sulfides such as pyrite, chalcopyrite, sphalerite, galena, scheelite, natural gold, electrum and calaverite; (3) the last is the barren quartz–carbonate stage, composed of quartz, calcite, and a small amount of pyrite.

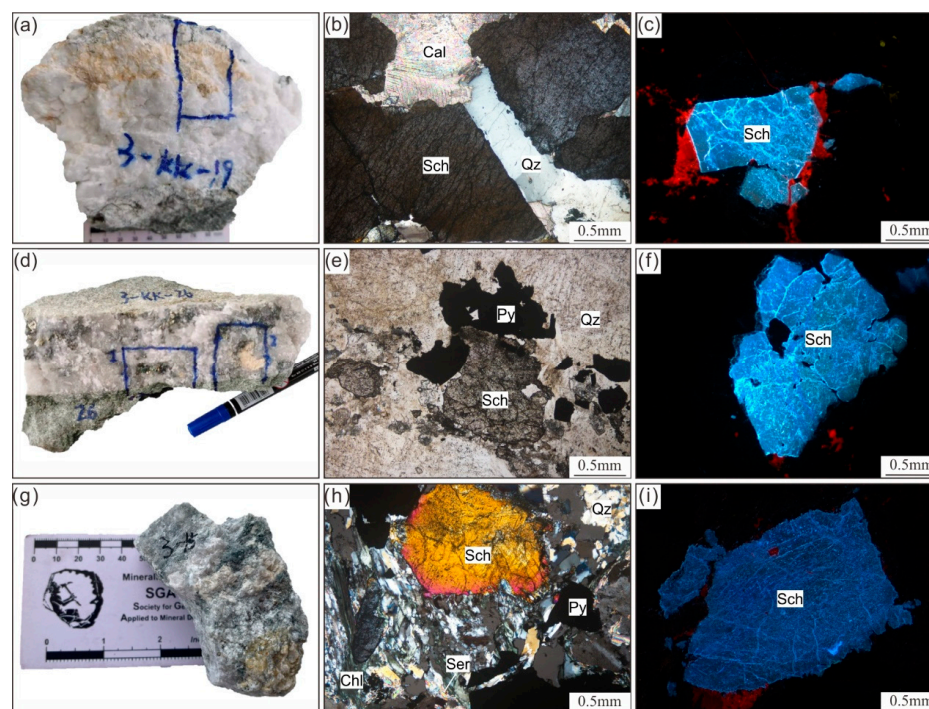


Figure 3. Characteristics of scheelites from different ores of the Doranasai gold deposit. (a–c) scheelite in early-stage milky quartz veins; (d–f) scheelite in middle-stage quartz–polymetallic sulfide veins; (g–i) scheelite in altered albite veins; Py—pyrite; Sch—scheelite; Qz—quartz; Chl—chlorite; Ser—sericite; Cal—calcite.

4. Samples and Analytical Methods

4.1. Sample Characteristics

Scheelite samples in this study were collected from the No. II and No. III prospects of the Doranasai gold deposit. Three types of scheelite were distinguished in the samples examined (Figure 3). Type I scheelite occurs as anhedral crystals less than 20 mm in diameter and disseminates in early-stage milky quartz vein (samples 3-19, 3-18, 3-KK-19 and 9001-9) (Figure 3a–c). Type II scheelite occurs as subhedral crystals less than 10 mm in diameter and disseminated in middle-stage smoky quartz–polymetallic sulfide vein, showing intergrowth features with quartz, pyrite and gold (samples 3-KK-13, 3-KK-20, 3-KK-26 and 3-KK-26-6) (Figure 3d–f). Type III scheelite is characterized by relatively fine-grained (0.5 to 2 mm in diameter) crystals in altered albite granite dyke (samples 3-9 and 3-15) (Figure 3g–i).

4.2. Analytical Methods

SEM, cathodoluminescence, and backscatter images were taken in the Guangzhou Tuoyan Testing Technology Co., Ltd., China. The scanning electron microscope model was TESCAN MIRA 3, and the working electric field voltage was 10.0–15.0 kV. The main element content of the mineral was obtained by the energy spectrum. The model was EDAX. The detection voltage of the energy spectrum was 20–25 kV and the working distance was 15–16 mm.

The EMPA data of the scheelite were completed at the Shandong Academy of Geological Sciences, and the instrument model was JEOL JXA8100. The experimental conditions were as follows: accelerating voltage 15 kV; beam current 12 Na; beam spot 5 mm; counting time 10–30 s; and the analytical accuracy of all elements was better than 1.5%. Taking natural minerals and synthetic oxides as standards, the data were corrected based on the ZAF program.

The trace element analysis of scheelite was performed using LA-ICP-MS in the laboratory of Guangzhou Tuoyan Detection Technology Co., Ltd., China. The ArF excimer laser ablation system (193 nm wavelength) was coupled with Agilent 7500a ICP-MS and a 1 m transmission tube. Helium was used as a carrier gas and argon as a make-up gas mixed with a carrier gas through the T-joint before entering the ICP. The maximum signal intensity was obtained by ablating the NIST srm610 test while maintaining a low ratio of ThO/Th (0.1–0.3%) and Ca²⁺/Ca⁺ (0.4–0.7%) to reduce the interference of oxides and double-charged ions. When ablating NIST srm610, the ²³⁸U/²³²Th ratio used as a complete vaporization indicator remained around 1. A micro flow PFA-100 self-priming Teflon atomizer was used for solution ICP-MS analysis. Each sample LA-ICP-MS analysis included a background acquisition of about 30 s, and then 50 s of data. NIST SRM 610 analysis was performed for every eight samples of beam spot analyses to correct the time-dependent drift of ICP-MS sensitivity and mass resolution [43]. The reference glass (MPI-DING) detection interluded before and after sample analysis.

The in situ Sr isotope of scheelite was carried out using LA-MC-ICP-MS in the National Geological Experiment Center of the Chinese Academy of Geological Sciences. An excimer laser ablation system (Australian scientific instruments and Resonics) with a resolution of 193 nm was used, which was equipped with an M-50 laser ablation cell (Lauren Technology Ltd. and Australian National University) and coupled with a Nu plasma HR MC-ICP-MS instrument (Nu Instruments, North Wales, UK).

5. Results

The results of the EMPA data for the major elements of the scheelite samples are shown in Table 1. The CaO content ranged from 19.44 to 19.64 wt% (average 19.56 wt%) for type I scheelite, from 19.41 to 19.83 wt% (average 19.62 wt%) for type II scheelite, and from 19.64 to 19.65 wt% (average 19.65 wt%) for type III scheelite. The WO₃ content ranged from 79.97 to 80.60 wt% (average 80.24 wt%) for type I scheelite, from 79.67 to 80.75 wt% (average 80.19 wt%) for type II scheelite, and from 80.28 to 81.02 wt% (average 80.65 wt%)

for type III scheelite (Table 1). Most of the other components were negligible, except for MoO_3 , which averaged 0.06 and 0.15 wt% for type I scheelite, 0.06 and 0.29 wt% for type II scheelite, and 0.16 wt% for type III scheelite (Table 1). Therefore, the three types of scheelite had similar EMPA results for the major elements.

The results of the LA-ICP-MS analyses for the REE and trace elements of the scheelite samples are shown in Table 2. Type I scheelite had ranges of ΣREE from 261 to 626 ppm (average 454 ppm), LREE/HREE (note LREE = La to Eu; HREE = Gd to Lu) ratios from 0.79 to 2.05 (average 1.61), δEu from 1.34 to 1.70 (average 1.49), Cr from 0.053 to 83.4 ppm (average 22.7 ppm), Sr from 848 to 1366 ppm (average 1126 ppm), Mo from 56.3 to 268 ppm (average 135 ppm), and Pb from 19.0 to 33.6 ppm (average 24.7 ppm). Type II scheelite had ranges of ΣREE from 350 to 6263 ppm (average 1340 ppm), LREE/HREE ratios from 1.14 to 4.06 (average 2.23), δEu from 1.15 to 2.54 (average 1.74), Cr from 2.65 to 1938 ppm (average 314 ppm), Sr from 742 to 3138 ppm (average 1332 ppm), Mo from 41.8 to 658 ppm (average 144 ppm), and Pb from 25.7 to 310 ppm (average 85.2 ppm). Type III scheelite had ΣREE ranges from 350 to 613 ppm (average 482 ppm), LREE/HREE ratios from 1.28 to 1.49 (average 1.39), δEu from 1.34 to 1.86 (average 1.60), Cr from 0.672 to 62.2 ppm (average 31.4 ppm), Sr from 960 to 1210 ppm (average 1085 ppm), Mo from 29.9 to 222 ppm (average 126 ppm), and Pb from 31.4 to 35.2 ppm (average 33.3 ppm).

The three types of scheelite had seagull-shaped chondrite-normalized [44] REE patterns and positive Eu anomalies (Figure 4). The REE patterns of scheelite were characterized by MREE enrichment, which is similar to Archaean gold deposits from Western Australia but different from Donggele granodiorite in the ore district (Figure 4) [11]. The scheelite from the Doranasai gold deposit had a ΣREY range of 404–7976 ppm, which was higher than that of Donggele granodiorite and albite granite dyke, and also higher than the Woxi Au-Sb-W deposit in Western Hunan ($\Sigma\text{REY} = 40.5\text{--}124$ ppm) [21] and the Nanyangtian W-polymetallic deposit in southeast Yunnan ($\Sigma\text{REY} = 96.1\text{--}252$ ppm) [45], but similar to the Archaean gold deposits in Western Australia ($\Sigma\text{REY} = 288\text{--}4377$ ppm) [11].

The results of the in situ Sr isotope data of the scheelite samples are shown in Table 3. The $^{87}\text{Sr}/^{86}\text{Sr}$ ratios of type I scheelite were between 0.704820 and 0.708606 (average 0.706111), while those of type II scheelite were between 0.705041 and 0.708047 (average 0.706582), showing similar $^{87}\text{Sr}/^{86}\text{Sr}$ ratios between the early and middle stages. To evaluate the source of the fluids and metals, the Sr isotope ratios of the scheelite were calculated at 291 Ma [5], and reported as $I_{\text{Sr}}(291\text{Ma})$. The Rb content of scheelite in each stage was very low, while the Sr content was high. The Rb/Sr ratio ranged from 0.00002 to 0.00151. The $I_{\text{Sr}}(291\text{Ma})$ values of type I scheelite ranged from 0.704820 to 0.708606, with an average of 0.706111, lower than that of type II scheelite, which had $I_{\text{Sr}}(291\text{Ma})$ values of 0.705041 to 0.708046 (average 0.706580). Thus, the $^{87}\text{Sr}/^{86}\text{Sr}$ ratio of scheelite measured in the Doranasai gold deposit was equivalent to the $I_{\text{Sr}}(291\text{Ma})$.

Table 1. Contents of major oxides of scheelite samples from the Doranasai gold deposit (wt%).

Sample	3-19B	3-18T	3-KK-19B	9001-9B	3-18B	3-kk-13B	3-kk-20-2B	3-kk-26T	3-kk-26-2T	3-kk-20-1T	3-KK-20-2T	3-kk-20-2T-1	3-kk-26B	3-kk-26-6B	3-9T	3-15T
Ore Type	Type I						Type II						Type III			
CaO	19.57	19.64	19.44	19.56	19.61	19.54	19.53	19.79	19.83	19.73	19.53	19.61	19.65	19.41	19.64	19.65
WO ₃	79.97	80.60	79.97	80.15	80.51	79.67	79.72	80.75	79.91	80.06	79.91	80.54	80.42	80.72	81.02	80.28
MoO ₃	0.06	0.09	0.15	-	0.10	0.16	0.17	0.06	-	-	0.22	0.29	-	-	-	0.16
FeO	-	0.03	-	-	-	-	0.08	0.01	0.04	0.02	-	-	-	0.06	-	-
MnO	0.04	-	0.02	0.01	-	-	0.07	0.03	0.02	-	-	0.01	-	0.03	-	0.01
PbO	0.03	-	-	-	-	-	0.13	0.15	0.23	-	-	-	-	-	-	0.07
ZnO	0.12	-	-	0.19	-	-	-	0.05	0.04	-	0.07	-	-	-	-	-
Total	99.79	100.36	99.57	99.91	100.23	99.37	99.70	100.84	100.08	99.81	99.73	100.45	100.07	100.22	100.66	100.16

Table 2. Representative trace element compositions of scheelites from the Doranasai gold deposit (ppm).

Sample No.	3-19B	3-18T	3-KK-19B	9001-9B	3-18B	3-19J	3-KK-13B	3-KK-20-2B	3-KK-26T	3-KK-26-2T	3-KK-13T	3-KK-20-1T	3-KK-20-2T	3-KK-20-2T-1	3-KK-26B	3-KK-26-6B	3-9T	3-15T
Ore Types	Type I						Type II						Type III					
Li	0.119	0.070	0.145	-	-	0.128	1.21	0.236	-	0.657	0.632	0.344	1.36	0.089	0.223	2.01	0.314	-
B	0.200	0.000	0.372	-	0.136	0.598	0.053	0.116	0.320	0.081	0.342	0.635	0.114	0.311	0.325	4.82	0.134	0.487
V	0.128	0.134	0.843	0.404	1.56	0.094	0.795	0.283	0.135	0.159	0.722	1.05	5.18	0.732	0.424	40.5	0.139	0.241
Cr	83.4	0.234	24.1	0.053	0.652	27.7	53.5	18.0	-	58.7	23.5	-	106	2.65	1938	0.672	62.2	
Co	0.024	0.019	0.051	0.065	0.017	-	0.018	0.113	-	0.101	0.103	0.138	0.311	0.011	0.041	0.151	0.109	0.039
Ni	0.411	0.446	0.575	0.397	0.300	0.480	0.275	0.241	0.467	0.383	0.808	0.969	2.16	0.590	0.186	2.06	0.277	0.436
Cu	-	0.053	-	-	0.041	0.041	0.014	0.056	-	0.040	0.095	0.110	-	0.102	0.040	0.393	-	0.007
Zn	0.029	-	0.010	-	0.005	0.051	-	0.085	-	0.464	0.093	0.418	-	0.204	-	10.7	0.004	0.127
As	4.65	3.70	18.9	5.57	7.58	3.91	6.13	3.27	1.35	4.25	9.00	8.77	24.5	6.88	12.7	2.68	2.55	11.6
Rb	0.011	0.003	0.017	0.013	0.007	0.012	0.018	0.492	0.039	0.022	0.011	0.028	0.043	0.043	0.042	37.7	0.021	0.008
Sr	848	1363	1056	1259	1366	864	742	950	1123	1334	814	2295	3138	999	1015	906	960	1210
Y	164	108	203	227	264	115	290	139	287	186	265	792	1713	163	387	196	246	125
Zr	2.14	2.00	2.37	1.97	3.81	1.86	2.61	2.08	2.11	2.13	2.33	8.89	16.8	1.86	2.03	5.12	2.68	2.12
Nb	0.615	0.859	0.958	0.502	0.993	0.518	0.561	0.385	0.633	1.25	0.542	1.99	4.60	0.380	1.21	1.39	0.449	0.715
Mo	254	98.5	77.6	56.3	58.3	268	52.0	46.3	70.0	55.3	59.2	361	658	56.7	41.8	43.0	29.9	222
Ag	-	0.003	0.012	0.009	0.003	0.006	-	-	0.003	0.009	-	-	-	-	-	0.024	0.013	0.008
Sn	0.043	0.093	0.108	0.053	0.144	0.011	0.034	0.041	0.128	0.043	0.154	0.331	0.692	0.125	-	0.672	-	-
Ba	0.115	0.041	0.853	0.276	0.337	0.201	0.085	0.319	0.056	0.050	0.883	1.21	0.099	1.37	0.549	115	0.163	0.551
La	2.81	6.74	10.3	17.8	14.7	5.41	60.3	17.0	27.5	8.32	16.6	69.6	449	17.1	20.2	24.4	10.7	4.92

Table 2. Cont.

Sample No.	3-19B	3-18T	3-KK-19B	9001-9B	3-18B	3-19J	3-KK-13B	3-KK-20-2B	3-KK-26T	3-KK-26-2T	3-KK-13T	3-KK-20-1T	3-KK-20-2T	3-KK-20-2T-1	3-KK-26B	3-KK-26-6B	3-9T	3-15T
Ore Types	Type I						Type II						Type III					
Ce	15.0	41.9	74.5	87.2	83.3	26.4	177	72.9	97.6	42.6	93.5	355	1565	84.7	110	95.4	61.2	27.0
Pr	4.92	13.1	24.1	21.6	23.6	7.96	40.3	17.6	18.6	11.7	26.7	98.3	319	22.0	30.1	15.9	18.8	8.89
Nd	47.6	106	186	143	178	68.1	264	116	100	92.0	195	765	1882	150	206	69.8	156	83.0
Sm	27.4	55.5	83.3	53.1	70.8	35.4	84.8	43.4	33.9	48.3	72.8	305	502	55.0	88.9	18.8	72.6	47.8
Eu	18.2	28.7	37.3	31.9	37.9	20.7	50.3	23.2	23.1	21.4	43.4	146	323	32.6	48.9	17.0	49.3	25.2
Gd	51.2	67.7	86.0	61.3	78.1	52.6	87.1	45.8	44.9	66.5	78.1	311	437	54.1	112	22.1	90.5	69.2
Tb	9.10	10.9	13.0	9.90	12.5	8.16	13.1	7.06	8.66	11.6	12.6	47.0	66.4	7.92	19.3	4.60	15.2	10.2
Dy	55.8	50.7	66.4	57.7	73.7	44.6	75.9	38.4	57.6	65.8	71.7	261	381	42.3	117	33.0	85.2	52.3
Ho	9.17	6.64	10.0	10.1	12.6	6.58	13.5	6.71	11.4	11.5	12.7	42.5	65.5	7.20	20.2	6.91	14.1	7.27
Er	15.2	10.0	17.8	22.1	26.1	10.5	29.5	15.4	30.1	24.3	29.0	89.4	152	16.0	44.8	19.3	26.9	10.8
Tm	1.08	0.71	1.60	2.38	2.71	0.76	3.11	1.77	3.81	2.58	2.98	9.34	18.0	1.76	4.61	2.88	2.47	0.77
Yb	3.18	2.15	5.46	11.0	10.5	2.04	13.6	8.29	21.5	11.2	13.0	42.8	96.0	8.08	21.0	17.9	10.0	2.48
Lu	0.189	0.147	0.388	0.947	0.843	0.121	1.32	0.816	2.45	1.08	1.19	4.10	8.98	0.772	2.01	2.04	0.770	0.159
Hf	0.022	0.020	0.018	0.022	0.020	0.015	0.031	0.022	0.035	0.041	0.023	0.093	0.118	0.013	0.046	0.147	0.028	0.026
Ta	0.020	0.011	0.021	0.006	0.014	0.013	0.014	0.014	0.016	0.020	0.018	0.079	0.125	0.012	0.025	0.056	0.009	0.006
Au	0.092	0.100	0.139	0.119	0.105	0.092	0.104	0.104	0.097	0.093	0.112	0.306	0.361	0.169	0.102	0.152	0.153	0.143
Bi	0.004	0.007	-	0.008	0.004	-	0.009	0.006	0.005	-	0.015	0.038	0.258	0.012	0.016	0.018	0.010	0.023
Pb	19.0	24.9	23.3	33.6	26.9	20.6	25.7	47.2	33.6	38.6	27.9	191	310	53.2	35.3	54.7	35.2	31.4
Th	0.023	0.010	0.157	0.030	0.189	0.040	0.146	0.308	0.129	0.121	0.019	0.266	0.469	0.320	0.024	1.23	0.023	0.060
U	0.009	0.004	0.015	0.007	0.024	0.010	0.054	0.047	0.035	0.012	0.014	0.124	0.104	0.081	0.007	0.311	0.005	0.011
REE	261	401	616	530	626	289	914	414	481	419	670	2547	6263	499	845	350	613	350
REY	425	509	819	757	890	404	1204	553	768	605	935	3339	7976	662	1232	546	859	475
LREE/HREE	0.79	1.68	2.05	1.99	1.86	1.30	2.82	2.30	1.63	1.14	2.00	2.13	4.06	2.58	1.46	2.16	1.49	1.28
δEu	1.46	1.43	1.34	1.70	1.55	1.46	1.77	1.58	1.81	1.15	1.75	1.44	2.06	1.80	1.50	2.54	1.86	1.34

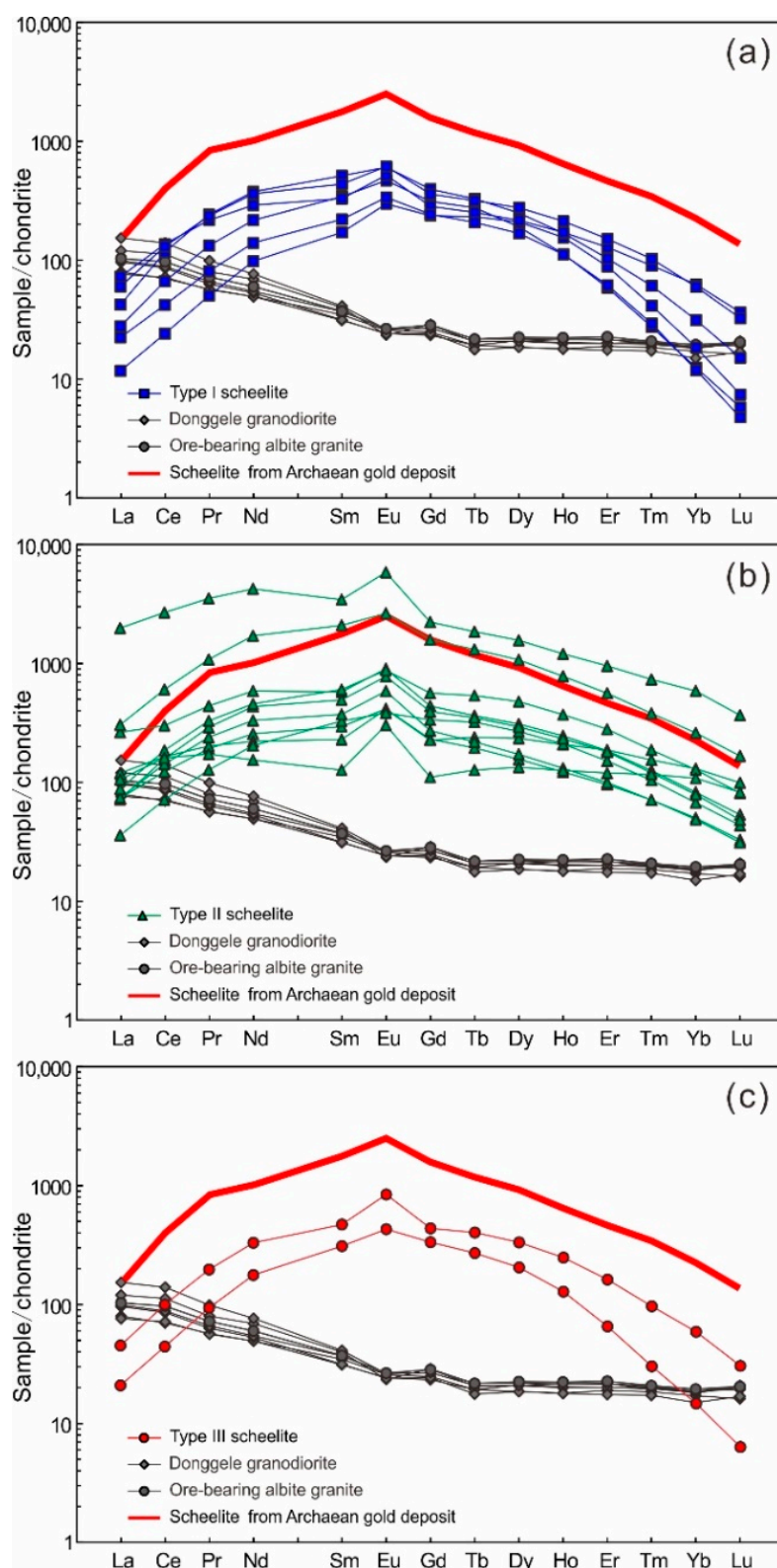


Figure 4. Chondrite-normalized REE patterns of scheelite from the Doranasai gold deposit. (a–c): three types of scheelite. Note: Scheelite from Archaean gold deposits, Western Australia is adopted from [11]. The data of Donggele granodiorite and ore-bearing albite granite dyke in Doranasai area are cited from [4]. The values of Chondrite are from [44].

Table 3. Results of in situ Sr isotopic analysis of scheelite from the Doranasai gold deposit.

Ore Types	Sample No.	Rb (ppm)	Sr (ppm)	$^{87}\text{Rb}/^{86}\text{Sr}$	$^{87}\text{Sr}/^{86}\text{Sr}$	2σ	I_{Sr} (291 Ma)	2σ
Type I	3-19-1	0.014	1160	0.000030	0.705380	0.000009	0.705380	0.000009
	3-19-2	0.007	1022	0.000020	0.705392	0.000009	0.705391	0.000009
	3-KK-19-1	0.031	1031	0.000090	0.705173	0.000001	0.705173	0.000001
	3-KK-19-2	0.007	869	0.000020	0.705202	0.000001	0.705202	0.000001
	3-KK-19-13-1	0.024	1096	0.000060	0.708606	0.000001	0.708606	0.000001
	3-KK-19-13-2	0.032	949	0.000100	0.707680	0.000001	0.707680	0.000001
	3-KK-19-13	0.005	775	0.000020	0.707308	0.000001	0.707308	0.000001
	3-KK-19-14	0.011	1018	0.000030	0.704820	0.000001	0.704820	0.000001
	3-KK-19-15	0.015	949	0.000040	0.705809	0.000001	0.705809	0.000001
	3-KK-19-16	0.005	775	0.000020	0.705822	0.000001	0.705822	0.000001
	9001-9-2	0.036	1432	0.000070	0.706475	0.000001	0.706474	0.000001
	9001-9-3	0.008	1077	0.000020	0.705669	0.000001	0.705668	0.000001
	Average ($N = 12$)					0.706111		0.706111
Type II	3-KK-13-1	0.036	782	0.000130	0.705507	0.000001	0.705506	0.000001
	3-KK-13-4	0.024	858	0.000080	0.705709	0.000001	0.705708	0.000001
	3-KK-13-5	0.018	736	0.000070	0.705041	0.000001	0.705041	0.000001
	3-KK-20-1-1	0.339	869	0.001130	0.705501	0.000001	0.705496	0.000001
	3-KK-20-1-2	0.492	942	0.001510	0.705617	0.000001	0.705611	0.000001
	3-KK-20-1-3	0.034	873	0.000110	0.705635	0.000001	0.705634	0.000001
	3-KK-20-1-4	0.086	897	0.000280	0.705419	0.000001	0.705418	0.000001
	3-KK-26-1	0.006	857	0.000020	0.706948	0.000001	0.706948	0.000001
	3-KK-26-2	0.028	777	0.000100	0.707338	0.000009	0.707338	0.000009
	3-KK-26-3	0.025	902	0.000080	0.707768	0.000001	0.707767	0.000001
	3-KK-26-4	0.011	923	0.000030	0.706998	0.000001	0.706998	0.000001
	3-KK-26-6-1-1	0.014	869	0.000050	0.707740	0.000008	0.707739	0.000008
	3-KK-26-6-2	0.033	979	0.000100	0.707518	0.000009	0.707517	0.000009
	3-KK-26-6-3	0.042	1011	0.000120	0.707938	0.000008	0.707937	0.000008
	3-KK-26-6-4	0.021	1598	0.000040	0.708047	0.000006	0.708046	0.000006
Average ($N = 15$)					0.706582		0.706580	

6. Discussion

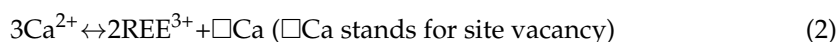
6.1. Redox State of Ore-Forming Fluids

The content of Mo in scheelite can indicate the redox properties of ore-forming fluids [24,27,28,46]. Mo⁶⁺ can substitute for W⁶⁺ in complete solid solution series between scheelite (CaWO₄) and powellite (CaMoO₄) due to their similar coordination number, ionic radii, and valence states [47]. Mo is transported as Mo⁶⁺ and enters scheelite by substituting W⁶⁺ under oxidizing conditions; however, when *f*O₂ decreases, Mo⁶⁺ is reduced to Mo⁴⁺ and precipitates as molybdenite (MoS₂) [46,48]. In the Doranasai gold deposit, the average Mo content of type I, II, and III scheelite is 135 ppm, 144 ppm, and 126 ppm, respectively. It is similar to typical orogenic gold deposits such as Sigma, Mt. Charlotte, and Daping gold deposits, which were probably formed under reducing conditions [11,15,26].

The ion radius of Ca²⁺ is 1.12 Å, while that of Eu²⁺ and Eu³⁺ in scheelite is 1.25 Å and 1.066 Å, respectively [47]. Therefore, both Eu²⁺ and Eu³⁺ can enter the scheelite lattice to replace Ca²⁺. However, because Eu²⁺ and Ca²⁺ have the same charge, Eu can relatively easily substitute the Ca of scheelite under reduction conditions, resulting in a positive abnormality of Eu. Different types of scheelite in the Doranasai gold deposit show positive Eu anomalies, indicating the relative reduction of ore-forming fluids. The positive Eu anomaly of scheelite in the Doranasai gold deposit may be related to the sericitization of plagioclase in the host-rock, because Eu and Ca are enriched in plagioclase and released during plagioclase sericitization, and are then uptaken by scheelite or carbonate (Figure 3h).

6.2. Ore-Forming Process Indicated by the REE Patterns

Scheelite from different ore systems and even different mineralization stages often show quite different REE compositions [49]. Because the ionic radii of trivalent REE (REY if Y is included) are similar to Ca²⁺, the REE³⁺ can substitute for Ca²⁺ in scheelite [49]. The REE characteristics of scheelite are strongly affected by charge balance and crystal structure. Two most important substitution mechanisms of REEs for Ca in scheelite are [49]:



Equation (1) requires the coupling substitution of charge balance compensation (Na⁺), while Equation (2) involves isomorphic substitution. Different substitution mechanisms affect the REE model of scheelite [24,49,50]. If Na is an element that provides charge balance, the ion radius of REE³⁺ that preferentially replaces Ca can be calculated according to Equation (1) [49]. Ghaderi et al. (1999) used the ion radius of [47] for coordination, and considered that MREE with ion radii close to 1.06 Å preferentially substituted the Ca position [49], which would cause MREE enrichment mode (bell shape). For Equation (2), Ca²⁺ in scheelite is replaced by REE³⁺ with a vacancy [49], which will reduce the hardness of the Ca site in scheelite and eliminate the limitation of the ion radius on the element substitute [24,28,49]. According to Coulomb's law, when the vacancy Ca is located between two REE substitution sites, the energy level of this substitution is minimized. Therefore, this process does not involve the preferential substitution of Ca²⁺ by MREE. The rare earth distribution pattern of MREE enrichment of scheelite in the Doranasai gold deposit indicates that REEs enter scheelite mainly through Equation (1). Therefore, REEs enter scheelite through the combination of REE³⁺ and Na⁺ to selectively replace Ca²⁺ in scheelite lattice in the form of valence compensation, indicating that they are mainly formed in Na-rich hydrothermal solutions. This is consistent with the scheelite in the gold deposits of the Kalgoorlie–Northman greenstone belt, Western Australia [49].

Mo, Bi, Sn, Nb and Ta can also enter the scheelite lattice due to their similar electronegativity to W [51]. The contents of Mo, Bi, Sn, Nb and Ta in the scheelite of the Doranasai gold deposit are relatively low, indicating that the ore-forming fluids may not be a high-temperature fluid formed by magmatic crystallization and differentiation. On the contrary, the CL characteristics and REE distribution patterns of scheelite are similar

to those of typical metamorphic hydrothermal gold deposits. For example, the Sr content in the scheelite of the gold deposits in Kalgoorlie and the Northman–Cambalda Archean greenstone belts (Western Australia) ranges from 341 to 4280 ppm, and the Mo content mainly ranges from 0.1 to 10 ppm, while the contents of Ba, Bi, Sn, Nb, Ta and other elements are generally less than 1 ppm [11]. Accordingly, the contents of rare elements in scheelite samples indicate that the ore-forming fluids of the Doranasai gold deposit should be metamorphic in origin.

6.3. Source of Ore-Forming Fluids

Based on the geochemical characteristics of fluid inclusions, Ridley and Diamond (2000) proposed that the Sr–Nd–Pb isotope can be used to trace the source of ore-forming fluids [52]. The Sr–Nd–Pb isotopes of ores have been successfully applied to trace the fluid sources of hydrothermal deposits [53–57]. For example, Kempe et al. (2001) studied the Sr–Nd isotopes of scheelite in the Muruntau gold deposit in western Tianshan and concluded that the ore-forming fluids had been sourced from the metamorphic devolatilization of sedimentary rocks [58]. Zhang et al. (2009) believe that the ore-forming fluids of the Yangshan gold deposit in Qinling Orogen are derived from the Bikou Group based on the Sr–Pb isotopic results of ore sulfides [55]; Niu et al. (2018) traced the ore-forming fluids using the Sr–Nd–Pb isotopes of ore sulfides and the wall–rocks of the Sarekuobu orogenic gold deposit and approved that the fluids were mainly derived from the ore-hosting Kangbutiebao Formation [59]. Abulimiti et al. (2021b) constrained the source of ore-forming fluids to the Altai Formation and diorite dykes by using sulfides and wall–rock Sr–Nd–Pb isotopes of the Tokuzbay gold deposit in the South Altai [60].

The $I_{Sr}(291Ma)$ averages of type I and type II scheelite from the Doranasai gold deposit were 0.706111 and 0.706580, respectively, which were higher than those of the Donggele granodiorite and the ore-bearing albite granite dyke. The Donggele granodiorite yielded $I_{Sr}(291Ma)$ values of 0.705385–0.706105, with an average of 0.705643, and the ore-bearing albite granite dyke yielded $I_{Sr}(291Ma)$ values of 0.704654–0.704735, with an average of 0.704695 [4]. Considering that ores are the products of interaction between host rocks and ore fluids, and the $I_{Sr}(291Ma)$ value of the ore-hosting albite granite dyke was obviously lower than those of the scheelite, we believe that the initial ore-forming fluids must have had higher $I_{Sr}(291Ma)$ values than the scheelite, i.e., higher than 0.706580 (Figure 5).

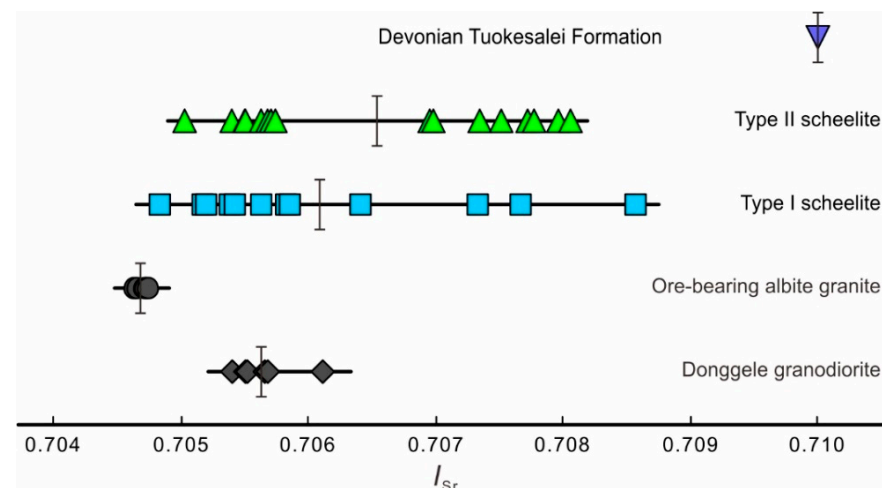


Figure 5. The $I_{Sr}(t)$ plot for the Doranasai gold deposit and related lithologies.

As mentioned above, the ore-hosting Tuokesalei Formation is composed of sedimentary rocks, intercalated with spilite–keratophyre assemblage whose $I_{Sr}(291Ma)$ ratio is up to 0.7100 [7]. As indicated by the Sr isotope system, the fluids forming the Doranasai deposit likely originated from the metamorphic devolatilization of the Tuokesalei Formation.

7. Conclusions

- (1) Three types of scheelite are recognized in the Doranasai gold deposit. They occur in milky quartz vein (type I), smoky quartz–polymetallic sulfide vein (type II), and altered albite granite dyke (type III);
- (2) The three types of scheelite have similar REEs and trace element characteristics, which are characterized by seagull-shaped REE patterns, positive Eu anomalies, high Sr concentrations and low Mo and As concentrations;
- (3) The geochemical characteristics of scheelite indicate that the REEs and other ore metals are derived from metamorphic fluids. The Eu anomalies and Mo concentrations of scheelite are obviously controlled by the redox conditions;
- (4) The gold mineralization may have originated from the metamorphic dehydration of the sedimentary sequence with the spilitite–keratoporphyry intercalation of the Tuokesalei Formation in South Altai.

Author Contributions: Field geological survey, X.L., A.A., X.H. and R.T.; writing—original draft, X.L., A.A. and X.H.; writing—review and editing, Y.C.; data analysis, X.L., A.A., X.H. and R.T. All authors have read and agreed to the published version of the manuscript.

Funding: This research was supported by the following funding agency: National Natural Science Foundation of China (Nos. U1803242 and 42072106) and the National Key Research and Development Program of China (2017YFC0601203).

Data Availability Statement: Data are available from the authors upon reasonable request.

Acknowledgments: We thank Western Region Gold Co., Ltd. and Habahe Huatai gold Co., Ltd. for their support in fieldwork. We sincerely thank Yanshuang Wu, Wenxiang Liu, Shen Han, Baicheng Huang, and Zhiwei Qiu for their help in the field sampling work. Guangzhou Tuoyan Detection Technology Co., Ltd., and the National Research Center of Geoanalysis have carried out rare earth and strontium isotope analysis of scheelite. Comments from the editor and two anonymous reviewers significantly enhanced the manuscript, which is appreciated very much by the authors.

Conflicts of Interest: The authors declare no conflict of interest.

References

1. Li, X.; Deng, X.H.; Liu, W.X.; Aibai, A.; Chen, X.; Han, S.; Wu, Y.S.; Chen, Y.J. Geology, fluid inclusion and H-O-C isotope geochemistry of the Doranasai gold deposit, Chinese Altai: Implications for ore genesis. *Int. J. Earth Sci.* **2021**, *1*–17. [[CrossRef](#)]
2. Nie, F.; Dong, G.C.; Zhang, Z.C. Composition and sulfur isotope characteristics of pyrite in Doranasai gold deposit, Xinjiang, and their significance. *J. Donghua Univ. Technol. (Nat. Sci. Ed.)* **2012**, *35*, 111–118.
3. Wu, F.; Cai, Y.B. Geological characteristics and metallogenic mechanism of Doranasai gold deposit, Xinjiang. *Xinjiang Nonferrous Met.* **2003**, *10*, 28–30.
4. Xiao, H.L.; Zhou, J.Y.; Wang, H.N.; Dong, Y.G.; Ji, J.F.; Zhao, Y. Geochemical characteristics and source of ore-forming fluids of Doranasai gold deposit, Xinjiang. *Chin. J. Geochem.* **2003**, *22*, 74–82.
5. Yan, S.H.; Chen, W.; Wang, Y.T.; Zhang, Z.C.; Chen, B.L. $^{40}\text{Ar}/^{39}\text{Ar}$ age of Irtysh gold metallogenic belt in Xinjiang and its geological significance. *J. Geol.* **2004**, *78*, 500–505.
6. Zhou, G.; Dong, L.H.; Qin, J.H.; Zhang, L.W.; Zhao, Z.H.; Li, Y. The formation age of granitoids and its constraints on gold mineralization in the Doranasai gold deposit, Xinjiang. *China Geol.* **2015**, *42*, 677–690.
7. Chen, H.Y.; Chen, Y.J.; Liu, Y.L. Metallogenesis of the Ertix gold belt, Xinjiang and its relationship to Central Asia-type orogenesis. *Sci. China Earth Sci.* **2001**, *44*, 245–255. [[CrossRef](#)]
8. Goldfarb, R.J.; Qiu, K.F.; Deng, J.; Chen, Y.J.; Yang, L.Q. *Orogenic Gold Deposits of China*; SEG Special Publications: Denver, CO, USA, 2019; Volume 22, pp. 263–324. [[CrossRef](#)]
9. Yin, Y.Q.; Li, J.X.; Guo, Z.L.; Hu, X.P. Classification of Altai gold deposit in Xinjiang and criteria for prospecting evaluation. *J. Guilin Inst. Technol.* **2005**, *25*, 141–145.
10. Bell, K.; Anglin, C.D.; Franklin, J.M. Sm-Nd and Rb-Sr isotope sytematics of scheelites: Possible implications for the age and genesis of vein-hosted gold deposits. *Geology* **1989**, *17*, 500–509. [[CrossRef](#)]
11. Brugger, J.; Maas, R.; Lahaye, Y.; McRae, C.; Ghaderi, M.; Costa, S.; Lambert, D.; Bateman, R.; Prince, K. Origins of Nd–Sr–Pb isotopic variations in single scheelite grains from Archaean gold deposits, Western Australia. *Chem. Geol.* **2002**, *182*, 203–225. [[CrossRef](#)]

12. Chen, L.; Qin, K.; Li, G.; Li, J.; Xiao, B.; Zhao, J. In situ major and trace elements of garnet and scheelite in the Nuri Cu–W–Mo deposit, South Gangdese, Tibet: Implications for mineral genesis and ore-forming fluid records. *Ore Geol. Rev.* **2020**, *122*, 103549. [[CrossRef](#)]
13. Fu, Y.; Sun, X.M.; Zhou, H.Y.; Lin, H.; Jiang, L.Y.; Yang, T.J. In-situ LA-ICP-MS trace elements analysis of scheelites from the giant Beiya gold-polymetallic deposit in Yunnan Province, Southwest China and its metallogenic implications. *Ore Geol. Rev.* **2017**, *80*, 828–837. [[CrossRef](#)]
14. McClenaghan, M.B.; Cabri, L.J. Review of gold and platinum group element (PGE) indicator minerals methods for surficial sediment sampling. *Geochem. Explor. Environ. Anal.* **2011**, *11*, 251–263. [[CrossRef](#)]
15. Sciuba, M.; Beaudoin, B.; Grzela, D.; Makvandi, S. Trace element composition of scheelite in orogenic gold deposits. *Miner. Depos.* **2020**, *55*, 1149–1172. [[CrossRef](#)]
16. Toverud, Ö. Dispersal of tungsten in glacial drift and humus in Bergslagen, southern Central Sweden. *J. Geochem. Explor.* **1984**, *21*, 261–272. [[CrossRef](#)]
17. Voicu, G.; Bardoux, M.; Stevenson, R.; Jebrak, M. Nd and Sr isotope study of hydrothermal scheelite and host rocks at Omai, Guiana Shield: Implications for ore fluid source and flow path during the formation of orogenic gold deposits. *Miner. Depos.* **2000**, *35*, 302–314. [[CrossRef](#)]
18. Frei, R.; Nägler, T.F.; Schönberg, R.; Kramers, J.D. Re-Os, Sm-Nd, U-Pb, and stepwise lead leaching isotope systematics in shear-zone hosted gold mineralization: Genetic tracing and age constraints of crustal hydrothermal activity. *Geochim. Cosmochim. Acta* **1998**, *62*, 1925–1936. [[CrossRef](#)]
19. Kent, A.J.R.; Campbell, I.H.; McCulloch, M.T. Sm-Nd systematics of hydrothermal scheelite from the Mount Charlotte Mine, Kalgoorlie, Western Australia; an isotopic link between gold mineralization and komatiites. *Econ. Geol.* **1995**, *90*, 2329–2335. [[CrossRef](#)]
20. Kozlik, M.; Gerdes, A.; Raith, J.G. Strontium isotope systematics of scheelite and apatite from the Felbertal tungsten deposit, Austria—Results of in-situ LA-MC-ICP-MS analysis. *Mineral. Petrol.* **2016**, *110*, 11–27. [[CrossRef](#)]
21. Peng, J.T.; Hu, R.Z.; Zhao, J.H.; Fu, Y.Z.; Yuan, S.D. REE geochemistry of scheelite in Woxi gold antimony tungsten deposit, Western Hunan. *Geochemistry* **2005**, *34*, 115–122.
22. Poulin, R.S.; McDonald, A.M.; Kontak, D.J.; McClenaghan, M.B. On the Relationship between Cathodoluminescence and the Chemical Composition of Scheelite from Geologically Diverse Ore-Deposit Environments. *Can. Mineral.* **2016**, *54*, 1147–1173. [[CrossRef](#)]
23. Poulin, R.S.; Kontak, D.J.; Andrew, M.; McDonald, A.; Beth, M.; McClenaghan, M.B. Assessing Scheelite as an Ore-deposit Discriminator Using Its Trace-element REE Chemistry. *Can. Mineral.* **2018**, *56*, 265–302. [[CrossRef](#)]
24. Song, G.X.; Qin, K.Z.; Li, G.M.; Evans, N.J.; Chen, L. Scheelite elemental and isotopic signatures: Implications for the genesis of skarn-type W–Mo deposits in the Chizhou area, Anhui Province, eastern China. *Am. Mineral.* **2014**, *99*, 303–317. [[CrossRef](#)]
25. Sun, K.K.; Chen, B. Trace elements and Sr–Nd isotopes of scheelite: Implications for the W–Cu–Mo polymetallic mineralization of the Shimensi deposit, South China. *Am. Mineral.* **2017**, *102*, 1114–1128.
26. Xiong, D.X.; Sun, X.M.; Shi, G.Y.; Wang, S.W.; Gao, J.F.; Xue, T. Characteristics and significance of trace elements, rare earth elements and Sr–Nd isotopic compositions of scheelite in Daping gold mine, Yunnan Province. *Acta Petrol. Sin.* **2006**, *22*, 733–741.
27. Yuan, L.L.; Chi, G.X.; Wang, M.Q.; Li, Z.H.; Xu, D.R.; Deng, T.; Geng, J.Z.; Hu, M.Y.; Zhang, L. Characteristics of REEs and trace elements in scheelite from the Zhuxi W deposit, South China: Implications for the ore-forming conditions and processes. *Ore Geol. Rev.* **2019**, *109*, 585–597. [[CrossRef](#)]
28. Song, G.X.; Cook, N.; Li, G.M.; Qin, K.Z.; Ciobanu, C.; Yang, Y.H.; Xu, Y.X. Scheelite geochemistry in porphyry-skarn W–Mo systems: A case study from the Gaojiabang deposit, East China. *Ore Geol. Rev.* **2019**, *113*, 103084. [[CrossRef](#)]
29. Chen, Y.J.; Pirajno, F.; Wu, G.; Qi, J.P.; Xiong, X.L.; Zhang, L. Epithermal deposits in north Xinjiang, NW China. *Int. J. Earth Sci.* **2012**, *101*, 889–917. [[CrossRef](#)]
30. Yang, F.; Geng, X.; Wang, R.; Zhang, Z.; Guo, X. A synthesis of mineralization styles and geodynamic settings of the Paleozoic and Mesozoic metallic ore deposits in the Altay Mountains, NW China. *J. Asian Earth Sci.* **2018**, *159*, 233–258. [[CrossRef](#)]
31. Windley, B.F.; Kroner, A.; Guo, J.H.; Qu, G.S.; Li, Y.Y.; Zhang, C. Neoproterozoic to Paleozoic geology of the Altai orogeny, NW China: New zircon age data and tectonic evolution. *J. Geol.* **2002**, *110*, 719–737. [[CrossRef](#)]
32. Zou, T.R.; Cao, H.Z.; Wu, B.Q. Orogenic and anorogenic granitoids of Altai mountains of Xinjiang and their discrimination criteria. *Acta Geol. Sin.* **1989**, *2*, 45–64.
33. Tong, Y.; Wang, T.; Jahn, B.M.; Sun, M.; Hong, D.W.; Gao, J.F. Post-accretionary Permian granitoids in the Chinese Altai orogeny: Geochronology, petrogenesis and tectonic implications. *Am. J. Sci.* **2014**, *314*, 80–109. [[CrossRef](#)]
34. Wang, T.; Hong, D.W.; Jahn, B.M.; Tong, Y.; Wang, Y.B.; Han, B.F.; Wang, X.X. Timing, petrogenesis, and setting of Paleozoic syn-orogenic intrusions from the Altai Mountains, northwest China: Implications for the Tectonic evolution of an accretionary orogeny. *J. Geol.* **2006**, *114*, 735–751. [[CrossRef](#)]
35. Broussolle, A.; Sun, M.; Schulmann, K.; Guy, A.; Aguilar, C.; Štípská, P.; Jiang, Y.; Yu, Y.; Xiao, W. Are the Chinese Altai “terrane” the result of juxtaposition of different crustal levels during Late Devonian and Permian orogenesis? *Gondwana Res.* **2019**, *66*, 183–206. [[CrossRef](#)]
36. Zheng, Y.; Zhang, L.; Chen, Y.J.; Qin, Y.J.; Liu, C.F. Geology, fluid inclusion geochemistry, and $^{40}\text{Ar}/^{39}\text{Ar}$ geochronology of the Wulasigou Cu deposit, and their implications for ore genesis, Altai, Xinjiang, China. *Ore Geol. Rev.* **2012**, *49*, 128–140. [[CrossRef](#)]

37. Zheng, Y.; Zhang, L.; Chen, Y.J.; Hollings, P.; Chen, H.Y. Metamorphosed Pb-Zn-(Ag) ores of the Keketale VMS deposit, NW China: Evidence from ore textures, fluid inclusions, geochronology and pyrite compositions. *Ore Geol. Rev.* **2013**, *54*, 167–180. [[CrossRef](#)]
38. Abulimiti, A.; Deng, X.; Pirajno, F.; Han, S.; Liu, W.; Li, X.; Chen, X.; Wu, Y.; Bao, Z.; Chen, Y. Geology and geochronology of the Tokuzbay gold deposit in the Chinese Altai: A case study of collision-related orogenic gold deposits in Central Asian Orogenic Belt. *Ore Geol. Rev.* **2021**, *136*, 104261.
39. Shen, Y.C.; Shen, P.; Li, G.M.; Zeng, Q.D.; Liu, T.B. Study on structural ore control law of Irtysh gold belt in Xinjiang. *Deposit Geol.* **2007**, *26*, 33–42.
40. Qin, K.Z.; Shen, M.D.; Tang, D.M. Mineralization type and diagenetic and metallogenic age of pegmatite type rare metals in Altai orogenic belt. *Xinjiang Geol.* **2013**, *31*, 1–7.
41. Wang, M.; Su, Q.Y.; Ma, J.B. Geological characteristics and genesis of deposit in Doranasai gold ore district. *Xinjiang Nonferrous Met. Suppl.* **2007**, *S2*, 6–8.
42. Li, H.Q.; Xie, C.F.; Chang, H.L. *Geochronology of Mineralization of Nonferrous and Precious Metal Deposits in Northern Xinjiang*; Geological Publishing House: Beijing, China, 1998; pp. 1–264.
43. Liu, Y.S.; Hu, Z.C.; Gao, S.; Günther, D.; Xu, J.; Gao, C.G.; Chen, H.H. In situ analysis of major and trace elements of anhydrous minerals by LA-ICP-MS without applying an internal standard. *Chem. Geol.* **2008**, *257*, 34–43. [[CrossRef](#)]
44. Sun, S.-S.; McDonough, W.F. Chemical and isotopic systematics of oceanic basalts: Implications for mantle composition and processes. In *Magmatism in the Ocean Basins*; Saunders, A.D., Norry, M.J., Eds.; Geological Society London Special Publications: London, UK, 1989; pp. 313–345.
45. Zeng, Z.G.; Li, C.Y.; Liu, Y.P. REE geochemical characteristics of two scheelite deposits of different genesis in Nanyang, Southeastern Yunnan. *Geol. Geochem.* **1998**, *26*, 34–38.
46. Rempel, K.U.; Williams-Jones, A.E.; Migdisov, A.A. The partitioning of molybdenum(VI) between aqueous liquid and vapour at temperatures up to 370 degrees C. *Geochim. Cosmochim. Acta* **2009**, *73*, 3381–3392. [[CrossRef](#)]
47. Shannon, R.D. Revised effective ionic radii and systematic studies of interatomic distances in halides and chalcogenides. *Acta Crystallogr.* **1976**, *A32*, 751–767. [[CrossRef](#)]
48. Linnen, R.L.; Williams-Jones, A.E. Evolution of aqueous-carbonic fluids during contact-metamorphism, wall-rock alteration, and molybdenite deposition at Trout Lake, British-Columbia. *Econ. Geol.* **1990**, *85*, 1840–1856. [[CrossRef](#)]
49. Ghaderi, M.J.; Palin, M.; Campbell, I.H. Rare earth systematics in scheelite from hydrothermal gold deposits in the Kalgoorlie-Norseman Region, Western Australia. *Econ. Geol.* **1999**, *94*, 423–438. [[CrossRef](#)]
50. Dostal, J.; Kontak, D.; Chatterjee, A. Trace element geochemistry of scheelite and rutile from metatubidite-hosted quartz vein gold deposits, Meguma Terrane, Nova Scotia, Canada: Genetic implications. *Mineral. Petrol.* **2009**, *97*, 95–109. [[CrossRef](#)]
51. Liu, Y.J.; Ma, D.S. *Tungsten Geochemistry*; Science Press: Beijing, China, 1987; pp. 45–120.
52. Ridley, J.R.; Diamond, L.W. Fluid chemistry of lode-gold deposits, and implications for genetic models. *Econ. Geol.* **2000**, *13*, 141–162.
53. Chen, Y.J.; Pirajno, F.; Sui, Y.H. Isotope geochemistry of the Tieluping silver-lead deposit, Henan, China: A case study of orogenic silver-dominated deposits and related tectonic setting. *Miner. Depos.* **2004**, *39*, 560–575. [[CrossRef](#)]
54. Barker, S.L.L.; Bennett, V.C.; Cox, S.F.; Norman, M.D.; Gagan, M.K. Sm-Nd, Sr, C and O isotope systematics in hydrothermal calcite-fluorite veins: Implications for fluid-rock reaction and geochronology. *Chem. Geol.* **2009**, *268*, 58–66. [[CrossRef](#)]
55. Zhang, L.; Yang, R.S.; Mao, S.D.; Lu, Y.H.; Qin, Y.; Liu, H.J. Sr-Nd isotopic composition characteristics and metallogenic material source of Yangshan gold deposit. *Acta Petrol. Sin.* **2009**, *25*, 2811–2822.
56. Ni, Z.Y.; Chen, Y.J.; Li, N.; Zhang, H. Pb-Sr-Nd isotope constraints on the fluid source of the Dahu Au-Mo deposit in Qinling Orogen, central China, and implication for Triassic tectonic setting. *Ore Geol. Rev.* **2012**, *46*, 60–67. [[CrossRef](#)]
57. Deng, X.H.; Chen, Y.J.; Santosh, M.; Yao, J.M.; Sun, Y.L. Re-Os and Sr-Nd-Pb isotope constraints on source of fluids in the Zhifang Mo deposit, Qinling Orogen, China. *Gondwana Res.* **2016**, *30*, 132–143. [[CrossRef](#)]
58. Kempe, U.; Belyatsky, B.V.; Krymsky, R.S.; Kremenetsky, A.A.; Ivanov, P.A. Sm-Nd and Sr isotope systematics of scheelite from the giant Au(-W) deposit Muruntau (Uzbekistan): Implications for the age and sources of Au mineralization. *Miner. Depos.* **2001**, *36*, 379–392. [[CrossRef](#)]
59. Niu, J.; Zheng, Y.; Zhang, L.; Yu, P.; Wang, Y.; Lai, C. Isotope geochemistry of the Sarekuobu metavolcanic-hosted gold deposit in the Chinese Altai (NW China): Implications for the fluid and metal sources. *Ore Geol. Rev.* **2018**, *100*, 51–62. [[CrossRef](#)]
60. Abulimiti, A.; Deng, X.; Pirajno, F.; Han, S.; Liu, W.; Li, X.; Chen, X.; Wu, Y.; Liu, J.; Chen, Y. Origin of ore-forming fluids of Tokuzbay gold deposit in the South Altai, northwest China: Constraints from Sr–Nd–Pb isotopes. *Ore Geol. Rev.* **2021**, *134*, 104165.